Acta Materialia 225 (2022) 117560

Contents lists available at ScienceDirect

Acta Materialia

journal homepage: www.elsevier.com/locate/actamat

Hall–Petch strengthening limit through partially active segregation in nanocrystalline Ag-Cu alloys

Frederic Sansoz [a,b,*], Xing Ke [a]

[a] Materials Science Program, The University of Vermont, Burlington, VT 05405, United States
[b] Department of Mechanical Engineering, The University of Vermont, Burlington, VT 05405, United States

ARTICLE INFO

Article history:
Received 12 October 2021
Revised 10 December 2021
Accepted 13 December 2021
Available online 15 December 2021

Keywords:
Hall–Petch limit
Nanocrystalline alloys
Solute segregation
Plasticity mechanisms
Atomistic simulation

ABSTRACT

The breakdown from grain-size strengthening to softening mechanisms is generally well understood for high-purity nanocrystalline materials when the mean grain size decreases to the nanometer range. In nanocrystalline alloys, however, the stabilization of nanosized grains by grain-boundary solute segregation complicates the above mechanisms. Moreover, current segregation models have little predictive power for determining the optimal solute content that maximizes Hall-Petch strengthening effects. In this article, using large-scale hybrid Monte-Carlo/molecular dynamic simulations, we present a systematic study of the Hall–Petch breakdown in Cu-segregated Ag alloys with grain sizes ranging from 8 nm to 59 nm, where three concentration-dependent regimes of plasticity are described: (1) Classical segregation strengthening behavior at low solute contents, (2) shear band-induced softening at high solute contents, and (3) a previously unknown, but extended plateau of maximum strengths for intermediate solute contents from 4 to 15 at.%, which we term as nanocrystalline *Sterling* silver. We find that flow strengths in nanocrystalline *Sterling* alloys naturally exhibit a zero-slope limit at the smallest grain sizes that is well below the ideal Hall–Petch strengthening trend. This phenomenon results from partially active grain-boundary segregation that acts to influence interfacial plasticity in some, but not all, grain boundary regions. Our findings amplify the atomic nature of solute segregation and interaction at grain boundaries and its complex roles on grain boundary-mediated plasticity mechanisms in nanocrystalline alloys.

1. Introduction

The concept of a "strongest" size in nanocrystalline (nc) materials was first brought up by Yip [1] to describe the critical grain size (d) at a maximum limit of strength, so called Hall–Petch breakdown, where deformation mechanisms transition from Hall–Petch grain-size strengthening [2,3] to grain-boundary (GB) induced softening, such as GB sliding [4,5], GB migration [6] and grain coarsening [7,8]. In nanostructured metallic alloys where conventional solid solution strengthening is generally found negligible [9–18], GB segregation of solute atoms gives rise to grain stability either by reducing the excess free energy or free volume of interfaces [19] or by forming fine clusters to pin the GB network [20]. From past experimental [21] and atomistic simulation [22] studies, controlling the stability of nanoscale grains by alloying has proven to be an effective strategy to displace the strongest size, or softening behavior, to the smallest grain sizes in nc metals. For instance, in nc Ni-W alloys [23,24] and Ni-P alloys [25,26], maximum hardness was measured at a grain size d between 7 nm and 9 nm after solute segregation, which is markedly smaller than the strongest size $d \sim 16$ nm in unalloyed nc Ni [27]. Likewise, record-breaking hardness values have been directly measured in nc Ni-Mo alloys with nanosized grains as small as $d = 10$ nm, while exhibiting continuous Hall–Petch strengthening without softening, owing to the increased GB stability from Mo segregation to GBs in Ni [21].

With rapid progress made in applying machine learning to atomistic modeling, it is now possible to inspect hundreds of nanocrystalline FCC, BCC and HCP binary alloys to qualitatively identify best candidates for GB segregation in polycrystals [28]. The new challenge, however, is to understand how solute concentration influences GB-strengthening mechanisms in the Hall–Petch breakdown regime [12]. On one hand, it has been well-documented experimentally that several nc binary alloys, such as Nb-doped Cu [29], Ti-doped Ni [30], Mg-doped Al [16] and Cu-doped Ag [18],

* Corresponding author at: Department of Mechanical Engineering, The University of Vermont, Burlington, VT 05405, United States.
E-mail address: frederic.sansoz@uvm.edu (F. Sansoz).

https://doi.org/10.1016/j.actamat.2021.117560

exhibit continuous segregation-induced GB strengthening with low-to-moderate solute contents, i.e. when the total solute is less than a few atomic percent. On the other hand, for higher solute contents ($\geq$ 10 at.%), GB embrittlement through shear localization failure has been observed in nc Ag-segregated Cu alloys [31] and nc Ni-segregated Al alloys [32]. In fact, an atomistic simulation study by Li and Szlusfarska [33] first pointed to a mechanism transition in nc Cu-Ag alloys where the flow strength increased at low Ag concentration, then decreased above 5.5 at.% Ag due to GB thickening into an amorphous Ag film, accompanied by reduced GB sliding resistance. They showed that this transition occurs over a range of grain sizes from 5 nm to 40 nm, which is crossing over the strongest size for this type of alloy. Likewise, another atomistic study by Li et al. [34] in nc Ni-Mo alloys reported a shift of GB-accommodated plastic deformation to dislocation-governed plasticity that avoided the occurrence of softening below the strongest size, by segregating Mo solute atoms. Also, the authors noted that the critical solute concentration at the transition was dramatically increased at the smallest grain size, due to increased GB atom fraction. In summary, all experimental and theoretical evidence points to a concentration limit where solute segregation can act as GB reinforcement, until the segregation effect reverses to strain localization-induced embrittlement. However, an unsettled question remains about understanding this concentration limit and its associated plasticity transition.

In this article, we use hybrid Monte-Carlo/molecular dynamics (MC/MD) simulations to fundamentally examine how solute concentration influences the strongest size and Hall–Petch breakdown mechanisms in Cu-segregated nc-Ag alloys with mean grain sizes ranging from 8 to 59 nm. We chose these alloys for several reasons. First, as synthesized in our past study [18], introducing trace concentrations of Cu is able to stabilize nc-Ag metals with a mean grain size of 50 nm at annealing temperatures up to 653 K. The GB segregation of Cu solute enables a combination of grain refinement and extreme nanoscale twinning in nc-Ag that gives rise to record-breaking strengths, in comparison to that of high-purity ultrafine-grained nanotwinned Ag [35]. To be consistent with past work, in this study, we investigate the plastic deformation behavior of nc-Ag polycrystals containing a constant nanotwin spacing (2.8 nm) and varying grain diameters (d). Second, because Ag and Cu have the highest electrical conductivity of all metals, adding elemental concentrations of Cu solute to Ag presents some clear advantages to maintain the conductivity, while breaking the conductivity-strength trade-off that is more commonly observed with heavily alloyed metals [18]. Third, past experimental studies on powder consolidated nc-Ag metals [36,37] have reported that a classical Hall–Petch hardening is holding down to a mean grain size of 17 nm. Apparently, in this grain size regime, the flow stress is predominantly controlled by the dislocation density and dislocation pile-ups, rather than by grain-size softening [38]. However, the compacting pressure and gas impurities with this processing method are known to affect the structure and density of the boundaries between the aggregates [39], which may influence the GB deformation mechanisms, requiring further study on stress-free structures of nc-Ag.

2. Computational methodology

Hybrid MC/MD simulations were performed to structurally and chemically relax large-scale nc-Ag polycrystals with different Cu concentrations similar to our previous methodology [17,18]. The software LAMMPS [40] was used with an embedded-atom method (EAM) potential for Ag-Cu binary alloys by Wu and Trinkle [41]. Our own simulations with this potential showed that the unstable and stable stacking-fault energies in pure Ag were equal to 115.3 mJ/m^2 and 16.6 mJ/m^2, respectively. We found that the generalized stacking-fault energy curve remained unchanged by randomly adding Cu atoms up to 5 at.% concentration, indicating that solid solution strengthening was absent up to this limit. A Voronoi tessellation scheme was applied for structure generation with randomly distributed grain centers, random crystallographic orientations, and fully periodic boundary conditions. GB atoms closer than 0.5 Å were removed. As shown in Fig. 1(a)–(c), several models with different mean grain sizes equal to 8, 10, 12, 16, 20, 25, 39, and 59 nm, were created in cubic simulation boxes of 30, 37.5, 45, 60, 48, 60, 60, and 90 nm in size, with a total of 1.5, 3.1, 5.3, 12.6, 6.5, 12.6, 12.6, and 42.6 million atoms, respectively. The mean grain size was computed with pure Ag polycrystals obtained after thermal equilibration at the segregation temperature, using the polyhedral template matching and grain segmentation analysis in the software Ovito [42]. The standard deviations for the models with 8 and 20 nm grain sizes were found to be equal to 1.1 and 2.1 nm after a 500 K relaxation, respectively. Because nc-Ag metals have shown a strong tendency to form nanoscale growth twins during sputter deposition [18], a uniform distribution of perfectly coherent twin boundaries with a spacing of 2.8 nm perpendicular to the [111] direction was added. This spacing was shown to facilitate GB-mediated plasticity in Cu-segregated nanotwinned Ag [17]. The energy of each model was minimized by the conjugate gradient method. The structure was then relaxed under zero pressure using an isothermal–isobaric (NPT) ensemble at 450 K for 100 ps, then cooled to 300 K in 50 ps, and held at the same temperature for another 50 ps. Temperature was rescaled every 500 steps. The timestep was 5 fs, which was found to conserve the total system energy.

The hybrid MC/MD approach used to simulate Cu atom segregation followed the method presented in [41]. It was run at 500 K for 1 million MD steps with a timestep of 2 fs and calls to MC every 10 MD steps. The temperature in MD was controlled by rescaling every 10 steps and pressure was maintained to 0 bar using a Berendsen barostat. The MC simulation part was carried out with a chemical potential difference $\Delta\mu = -2.5$ eV and a variance of Lagrange multiplier $\kappa = 100$. The target solute concentration was varied by 1 at.% intervals up to 20 at.% by prolonging the MC/MD cycles without changing the chemical potential difference. After segregation to the desired concentration, the model was relaxed again in NPT ensemble under zero pressure from 500 K to 300 K for 100 ps and kept at 300 K for another 100 ps.

The models were deformed in pure tension by stretching the simulation box at an engineering strain rate of 10^8 s^{-1} along the x-direction until 10% strain. NPT ensemble at 300 K and zero pressure applied laterally along the z and y directions were used. The average tensile stresses were computed by adding the corresponding Virial-theorem stress component over all atoms and dividing by the deformed volume of the simulation box. The flow stress was determined by averaging stresses over strains ranging from 7% to the maximum 10%, because the flow stress variation for each model was found to be smaller over this range. Plastic deformation mechanisms were studied by common neighbor analysis (CNA) and atomic strain analysis in OVITO.

To quantify GB properties, an algorithm using the Voronoi tessellation method [43] was developed to identify a list of GB atoms before deformation by creating a network of three-dimensional cells of $\sim$1 nm in wall thickness encompassing each GB interface in the models. Other related works tend to use the CNAto detect GB atoms instead. We did not use this approach, primarily because some Cu atoms remained randomly distributed inside the grains and did not segregate totally to the GBs, and during plastic deformation simulation, defect atoms in dislocation cores inside the grain interior could be mistakenly recognized as GB atoms by CNA.

Furthermore, we computed the excess free volume (EFV) per GB atom based on the approach proposed by Li and Szlufarska [33].

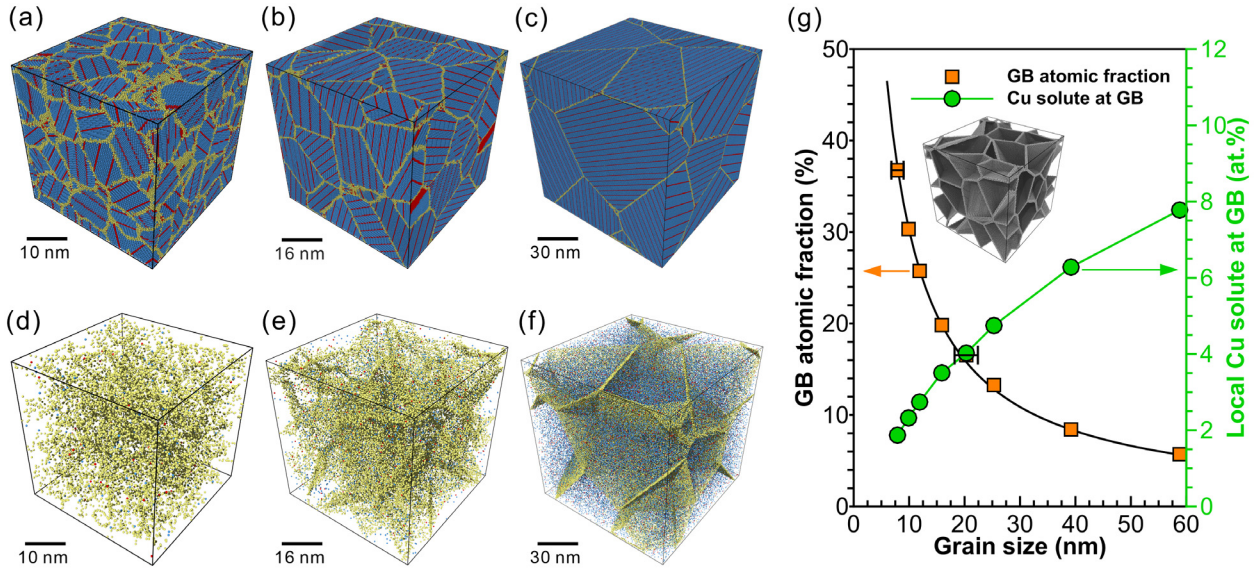

Fig. 1. Hybrid MC/MD simulations of solute segregation in nanocrystalline Ag-Cu alloys with a constant Cu content of 0.8 at.%. Microstructure snapshots for Ag models with a mean grain size of (a) 8 nm, (b) 20 nm and (c) 59 nm. Cu atom distribution at 500 K for a grain size of (d) 8 nm (e) 20 nm and (f) 59 nm. Atoms in perfect FCC arrangement are colored in blue, coherent TBs in red color, and grain boundaries (GBs) in yellow color. (g) GB atomic fraction and local GB solute concentration as a function of mean grain size. The inset shows the GB network region used for calculation in the 20 nm grain size model. See text for the fitting of GB atom fraction. Horizontal error bars represent the grain-size standard deviation obtained for pure nc-Ag models after a 500 K thermal relaxation. (For interpretation of the references to colour in this figure legend, the reader is referred to the web version of this article.)

Each atom inside the GB network was analyzed using the Voronoi modifier in OVITO to calculate its atomic volume. The EFV was calculated using the equation

$$EFV = \frac{\sum V_{GB} - N_{Ag} \times V_{Ag} - N_{Cu} \times V_{Cu}}{N_{Ag} + N_{Cu}} \quad (1)$$

where V_{GB} is the atomic volume for each atom inside GBs, N_{Ag} and N_{Cu} is the number of Ag and Cu atoms inside GBs, respectively, V_{Ag} and V_{Cu} are the atomic volumes of Ag and Cu atoms in the single crystalline phase, respectively. The atomic volume was calculated using the Voronoi modifier in OVITO. Also, we computed the atomic-level von-Mises effective stresses by averaging the six components of the virial stress tensor over all atoms within a spherical volume with a cutoff radius of 5.99 Å around each atom. The simulations were performed on the high-performance supercomputers at the Extreme Science and Engineering Discovery Environment (XSEDE) [44] and the National Energy Research Scientific Computing Center (NERSC).

3. Results and discussion

3.1. Dependence of GB segregation on grain size

Fig. 1 presents the influence of mean grain size (and GB atom fraction) on the equilibrium distributions of Cu solute atoms at 500 K in Ag polycrystals, with segregation fixed at a constant solute content of 0.8 at.% Cu, corresponding to the value studied previously at a large grain size of d = 59 nm [17,18]. Fig. 1(d)–(f) shows the formation of a homogeneous 3D network of GB solute atoms colored in yellow. Some Cu atoms are found distributed randomly at face-centered cubic and some hexagonal-close packed sites in the grain interior at d = 59 nm; however, these tend to disappear at smaller grain sizes. Cu solute atoms show no preference for segregation into coherent twin boundaries, because there are no twin boundary defects to form solute attraction sites, contrary to our previous simulations in [17].

The present atomistic simulations show a strong grain-size dependence of the solute content segregated to GBs, confirming past thermodynamic calculations [45]. In theory, the GB atom fraction for equiaxed polycrystals is equal to [46]:

$$f_{GB} = 1 - \left[\frac{d-t}{d}\right]^3 \quad (2)$$

with t the GB thickness. This equation matched well with our simulations in Fig. 1(g) when a constant t = 1.13 nm is chosen. At an 8-nm grain size, Fig. 1(d) shows that most Cu atoms are segregated inside GBs, where the local Cu content is equal to 1.9 at.% as indicated in Fig. 1(g). As the grain size is increased, however, Fig. 1(g) reveals that GBs are increasingly more concentrated with solute because the GB atom fraction decreases, while t remains approximately constant. Consequently, the local Cu solute at GBs reaches 7.8 at.%, i.e. ~10 times higher at GBs than the total concentration. Therefore, it can be concluded that the local Cu concentration in GBs after hybrid MC/MD simulation increases sharply with increasing grain size. This conclusion suggests that larger solute contents might be required at smaller grain sizes to maintain same strengthening efficiency from GB segregation.

3.2. Hall–Petch strengthening limit

The flow stress averaged over strains from 7 to 10% is represented in Fig. 2, as a function of grain size d and total Cu content up to 20 at.%. For pure nc-Ag (with 2.8 nm nanotwins), our atomistic simulations show a normal transition from Hall–Petch strengthening to grain-size softening, associated with a maximum strength of 1.5 GPa predicted at d = 20 nm. We obtained a least-square fit of the Hall–Petch equation:

$$\sigma = \sigma_0 + \frac{K}{\sqrt{d}} \quad (3)$$

where σ is the flow stress, σ_0 is the friction stress for dislocation motion, and K is the Hall–Petch grain-size hardening constant. For pure nc-Ag, the classical Hall–Petch relation holds well up to 20 nm and is in good agreement with past experimental observations made on powder consolidated nc-Ag metals [36,37]. For

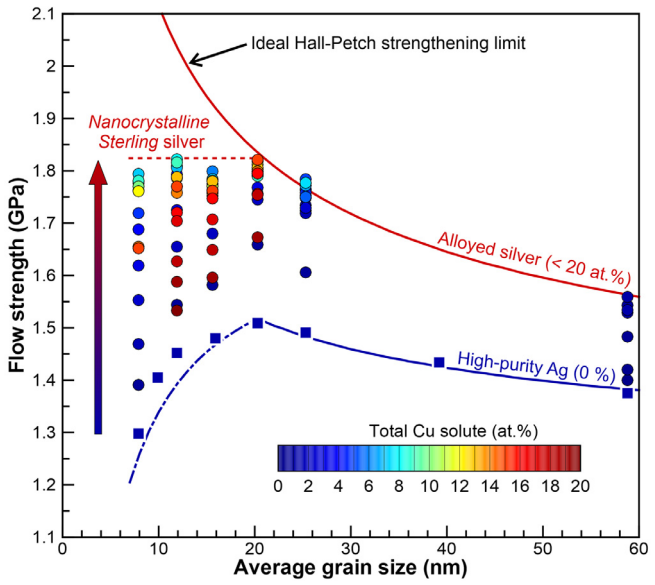

Fig. 2. Hall–Petch plot for nanocrystalline Ag-Cu alloys with total Cu solute contents up to 20 at.%. Pure Ag metals exhibit a classical Hall–Petch breakdown at an average grain size of 20 nm, whereas GB solute segregation strengthening is significant in Ag-Cu alloys. However, flow strengths in heavily segregated nanocrystalline Ag-Cu alloys present a saturation in the breakdown regime, suggesting that the ideal Hall–Petch strengthening limit is not always achievable with small grain sizes through conventional GB solute segregation. The amorphization model by Chandross and Argibay [47] for shear strength softening in pure Ag metals (0%) based on Eq. (3) is represented by a dotted-dashed line.

$d \leq 20$ nm, we compared the flow strength predicted by our simulations to the shear softening model based on amorphization of the GB region, rather than GB sliding, proposed by Chandross and Argibay [47], which is given by

$$\tau = \left(L\frac{\rho_L}{M}\right)\left(1 - \frac{T}{T_m}\right)(1 - f_{GB}) + \tau_0 \tag{4}$$

where $\tau = \sigma/\sqrt{3}$ is the shear strength for polycrystals, L is the heat of fusion, ρ_L is the density of the liquid at the melting temperature, M is the atomic mass, T is the temperature (300 K), T_m is the melting temperature and τ_0 is a stress threshold dependent on strain rate and temperature. We used Eq. (2) for the GB fraction f_{GB}. From past first-principles calculations for Ag [48], we used $L = 10.806$ kJ/mol, $\rho_L = 9.49$ g cm^{-3}, $M = 107.9$ g mol^{-1}, $T_m = 1209$ K, and by fitting to our MD results at $T = 300$ K, $\tau_0 = 0.475$ GPa. Both GB amorphization theory and atomistic simulation results show good agreement for grain sizes equal to 20 nm or smaller, further substantiating that the strongest size should be on the order of 20 nm in pure nc-Ag.

Fig. 2 indicates that the effect of Cu segregation on flow stresses in Ag polycrystals is quite dramatic, because an increase of strength by up to 48% is evidenced over the range of studied grain sizes (8–59 nm). This finding is significant in several aspects. First, by fitting Eq. (3) to data with only $d \geq 20$ nm, we find that the parameter σ_0 remains unchanged between pure nc-Ag and Cu-segregated nc-Ag models, 1.191 GPa and 1.176 GPa, respectively, which implies that Cu alloying did not significantly influence the stacking-fault energy for crystal slip in this type of alloy [49]. By contrast, after segregation, K increased by more than 100% from 1.47 to 2.97 GPa m$^{0.5}$. Li [50] attributed such a rise in the Hall–Petch slope during GB segregation to the pinning effect of impurities on GB dislocation sources and the local alteration of GB structure. In effect, some supplementary analysis is presented below to support Li's hypothesis and shows that the EFV decreases linearly with the local solute content at GBs, which has a significant influence on GB-assisted plasticity.

Second, it is worth noting in Fig. 2 that flow strengths in segregated models with $d \leq 20$ nm reach a maximum at 1.82 GPa, which is significantly smaller that the ideal Hall–Petch strengthening limit if we were to extend Eq. (3) to the smallest grain sizes. The maximum strength is almost constant for all $d \leq 20$ nm, implying that the underlying plasticity mechanism governing the zero-slope limit in the GB segregated models may be grain-size independent. However, it is established that GB sliding rates limited by GB diffusion exhibit a third-power law with respect to grain size in equiaxed polycrystals [51]. Therefore, we observe that the Hall–Petch limit in segregated Ag-Cu alloys possibly evades classical GB sliding mechanisms.

Third, a theory for estimating the effect of alloying on strongest size in nc alloys has been previously proposed by Schuh et al. [23]. Adapting this theory to the case of Cu solute in Ag polycrystals allows us to estimate that:

$$\frac{d_{alloy}}{d_{pure}} \approx \left[\frac{D_{Ag-Cu}}{D_{Ag}}\left(1 - X^{tot}\right) + X^{tot}\right]^{2/7} \tag{5}$$

where d_{alloy} and d_{pure} are strongest sizes in the segregated alloy and pure metal, respectively, $D_{Ag\text{-}Cu}$ is the diffusivity of Cu in Ag, D_{Ag} is the self-diffusivity of Ag, and X^{tot} is the total Cu content. However, the ratio $D_{Ag\text{-}Cu}/D_{Ag}$ is estimated to be only about 10^{-7} [52,53]. Therefore, Eq. (5) can be approximated to $d_{alloy}/d_{pure} \approx (X^{tot})^{2/7}$. Numerically, this estimate suggests that the strongest size should steadily decrease as solute content increases. For example, it could be reduced by half, from $d = 20$ nm to 10 nm, if $c = (0.5)^{7/2} = 8.8$ at.%. However, this theory is not consistent with results presented in Fig. 2, because maximum strength with 8 at.% Cu is reached at $d = 12$ nm, whereas the strongest size with 12 at.% Cu is found to be larger, $d = 20$ nm. Furthermore, for all models with $d \leq 20$ nm, Fig. 2 shows that the flow strengths increase to a maximum before decreasing for increasing Cu contents.

To better understand this phenomenon, the dependence of flow strength on Cu content is represented in Fig. 3 for the smallest grain size ($d = 8$ nm). From this figure, it is shown that flow strengths can be separated into three concentration-dependent plasticity regimes: (1) A classical segregation strengthening behavior at low solute contents up to 6 at.%, (2) an extended plateau of maximum strengths for intermediate solute contents, and (3) concentration-dependent softening for high solute content above 12 at.%. Interestingly, the plateau regime that corresponds to maximum strengths in nc Ag-Cu alloys, is reached for a range of solute contents that has not been well studied in the literature. Historically, *Sterling* Ag has been used for coins and jewelry in which at least 7.5 at.% Cu is added to harden it since pure Ag is too soft [54]. By analogy, we term the alloys with compositions lying within the plateau of maximum strengths in Fig. 2 as nc *Sterling* silver.

3.3. Segregation-induced strain localization and softening

To further investigate the underlying softening mechanism at higher Cu contents, MD snapshots of atomic von-Mises shear strain at yielding (from 0 to 4.5% applied strain) and during plastic flow deformation (from 7 to 9.5% applied strain) are represented in Fig. 4 for different Cu solute contents (0, 8 and 15 at.%). In Fig. 4, the onset of yielding is marked by dislocation nucleation at all concentrations, but the level of GB plasticity is more profoundly affected by the segregation. In pure nc-Ag, Fig. 4(a) shows that yielding is associated with GB sliding and dislocation nucleation simultaneously, whereas segregation in both Fig. 4(b) and (c) is found to dramatically reduce GB sliding at yielding. In comparing the two segregated models, GB atom shuffling is found to be slightly higher at 8 at.% Cu than 15 at.% Cu. Fig. 3(a), however, showed

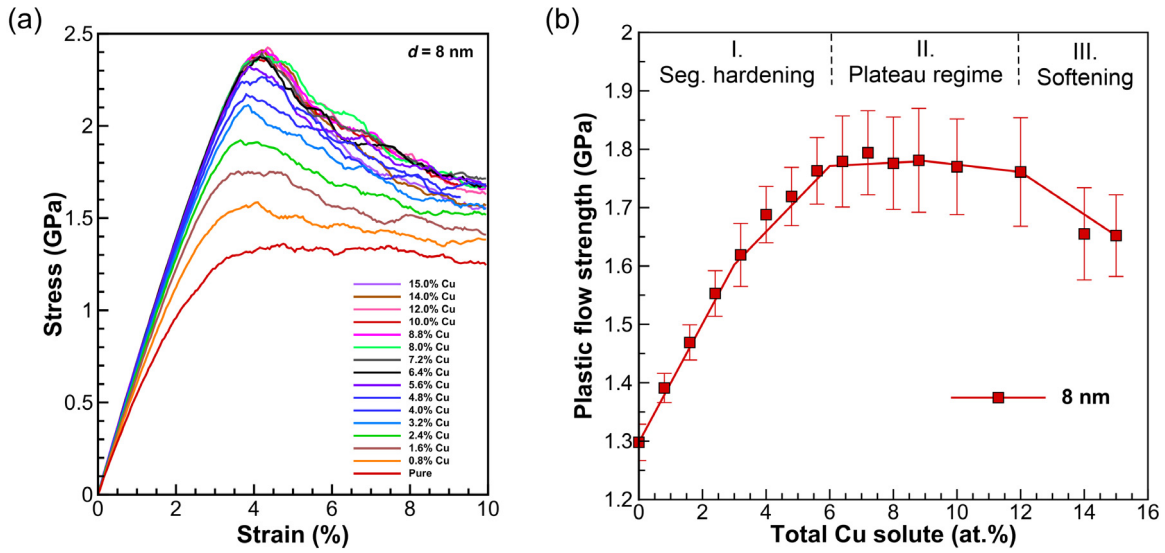

Fig. 3. Effect of total solute content on mechanical behavior in nanocrystalline Ag-Cu alloys with a mean grain size (d) of 8 nm. (a) Simulated tensile stress-strain curves. (b) Flow stresses averaged between 7 and 10% applied strain. The mechanical behavior of segregated alloys is divided into three regimes delineated by GB segregation strengthening, a plateau of constant stresses, and segregation softening.

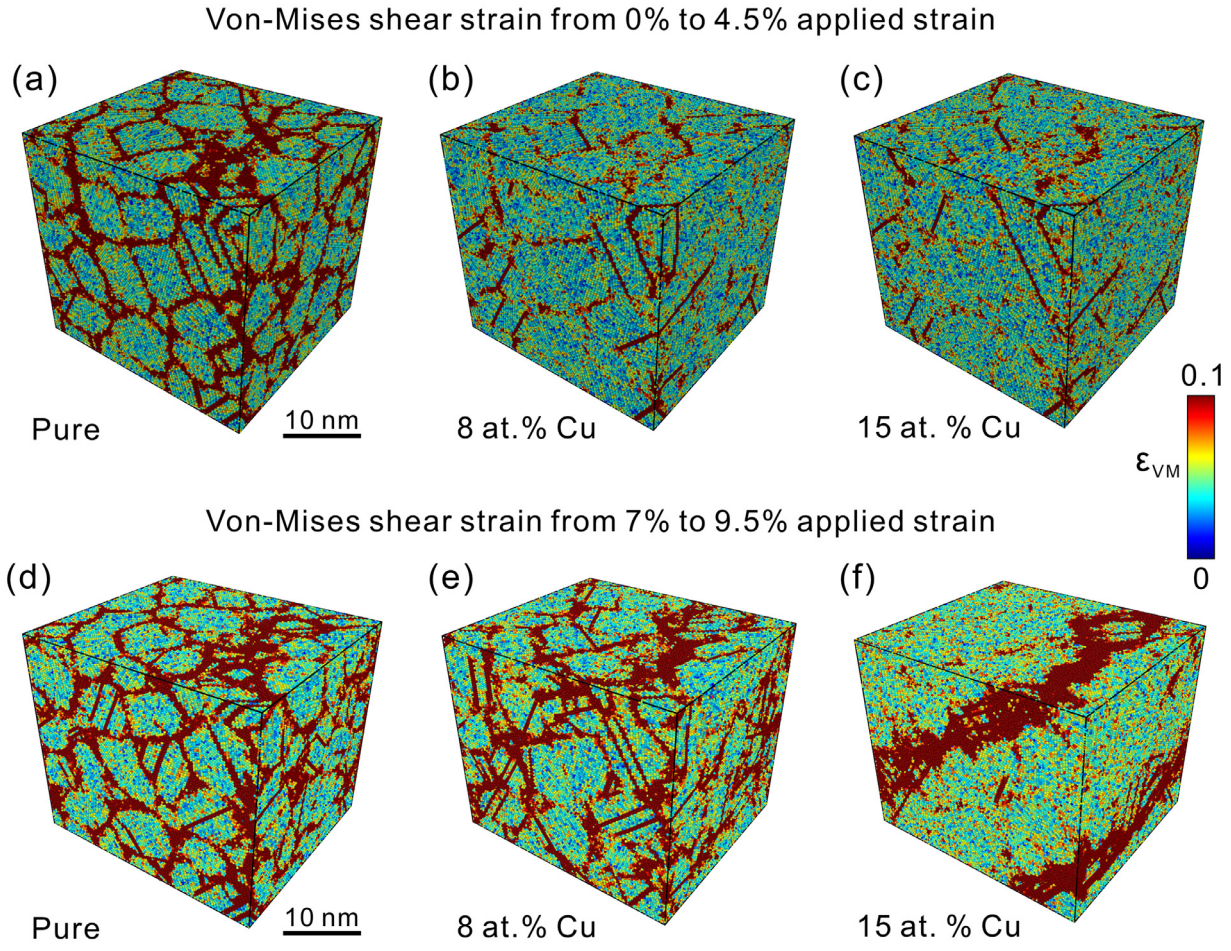

Fig. 4. Effect of total solute content on plastic strain localization in nanocrystalline Ag-Cu alloys (d = 8 nm). Local atomic von-Mises shear strains (ε_{VM}) are calculated in the same models at applied strains from (a)–(c) 0% to 4.5% and (d)–(f) 7% to 9.5%, respectively.

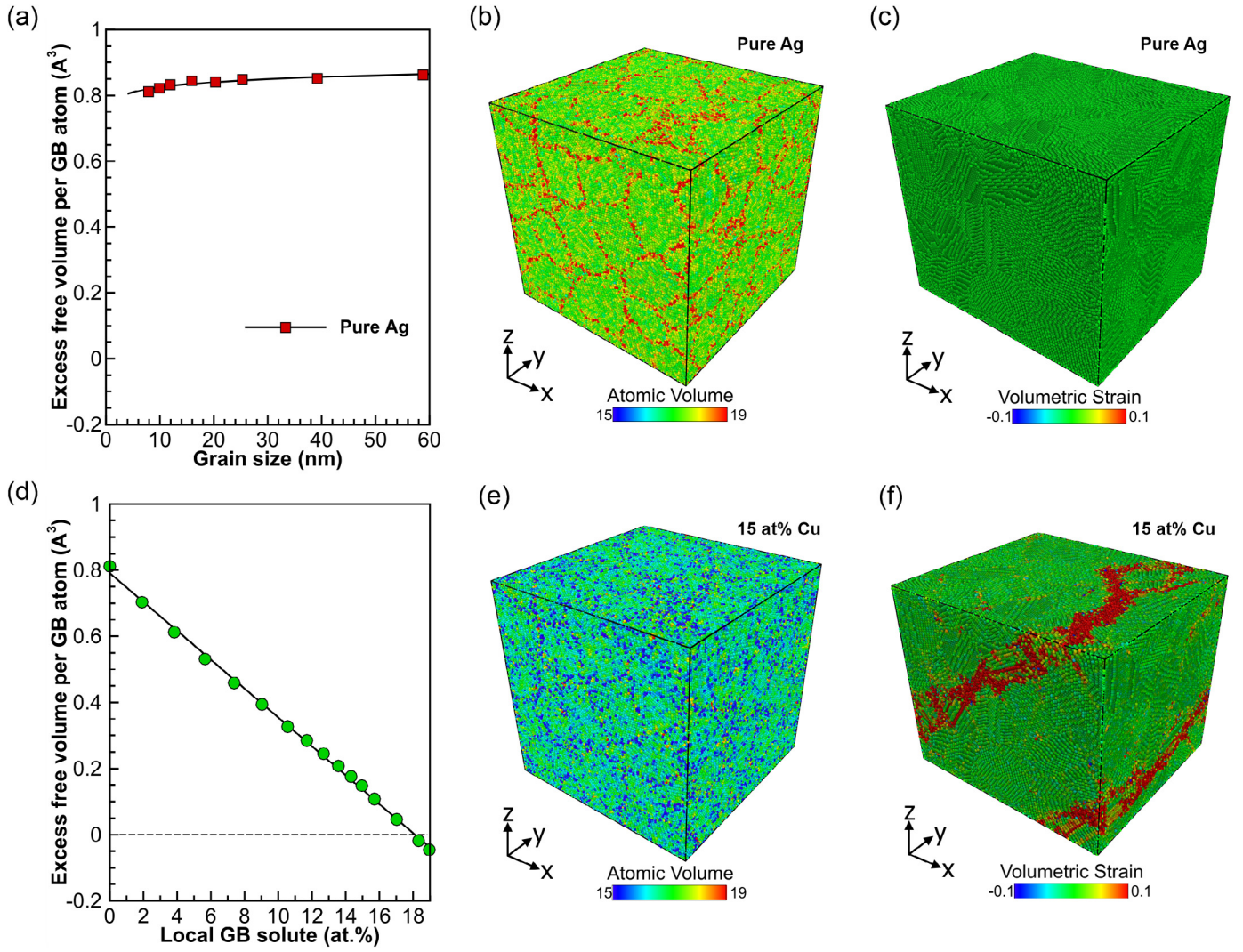

Fig. 5. Excess GB free volume in nanocrystalline Ag-Cu alloys. (a) Excess free volume per GB atom as a function of mean grain size. (b) Initial atomic volume (in Å) without solute for $d = 8$ nm. (c) Homogeneous volumetric strain at 9.5% strain without solute. (d) Excess free volume per GB atom as a function of local GB solute concentration for constant $d = 8$ nm. (e) Initial atomic volume (in Å) with 15 at.% Cu solute for $d = 8$ nm. (f) Nanovoid expansion along intense shear band at 9.5% strain with 15 at.% Cu solute.

that this difference had negligible effect on the peak of the stress-strain curves at a yield strain of 4.5%, relative to the sharp increase of stress observed when solute concentration was increased from 0 to 6 at.% Cu.

Furthermore, Fig. 4(d) shows no fundamental difference between the yielding and plastic flow mechanisms in pure nc-Ag. For Ni-W alloys, the amorphization theory by Chandross and Argibay [47] has been suggested to explain the crossover in behavior from crystal-like to amorphous-like deformation that was directly visible in experiments with decreasing grain size [55]. In Ag-Cu alloys, however, the effect of Cu content on GB plasticity mechanisms presented in Fig. 4 does not support this hypothesis because, as the Cu content is raised to 8 at.%, Fig. 4(d) shows that GB amorphization at $d = 8$ nm is significantly diminished compared to that in the pure nc-Ag model. In fact, past MD simulations by Ke et al. [18] have demonstrated that GB sliding is the predominant mechanism of GB plasticity in Cu-segregated nanotwinned-nanocrystalline Ag alloys. Also, Koju and Mishin [56] have calculated that GB atom diffusion of both Cu and Ag elements remains surprisingly high after segregation in Cu-Ag alloys. Furthermore, it is important to observe in Fig. 4(e) that GB-localized plasticity is only significantly reduced in some, but not all, GB regions.

Also, when the Cu content reaches 15 at.% in Fig. 4(f), the deformation mechanism dramatically changes to shear banding with intense strain localization through combined intergranular and intragranular slip, which is absent at yielding in Fig. 4(c). It is found that Cu segregation eliminates dislocation nucleation from GBs in grains adjacent to the shear band. In summary, the softening behavior associated with GB segregation of high solute contents ($>$ 12 at.%) relates to the formation of a localized shear band accompanied by a pronounced increase in the resistance to GB sliding and to GB-nucleated crystal slip.

It is possible to interpret the effects of high Cu content on both GB sliding and crystal slip in nc Ag-Cu alloys as follows. First, in nanocrystalline metals, the excess GB atom volume is known to influence GB sliding mediated by atom-shuffling and dislocation nucleation mechanisms [57–60]. In fact, Li and Szlusfarska [33] demonstrated that the EFV was a key parameter in the overall strength and GB stability of nc Cu-Ag alloys when Ag solute is segregated to GBs. In Fig. 5, we represent the EFV computed in our simulated Cu-segregated Ag polycrystals. Fig. 5(a) shows that the EFV is independent on grain size in pure Ag, where EFV takes a positive value of + 0.8 Å^3 per GB atom, i.e., consistent with a larger atom disorder in random GBs. As shown in Fig. 5(b), it im-

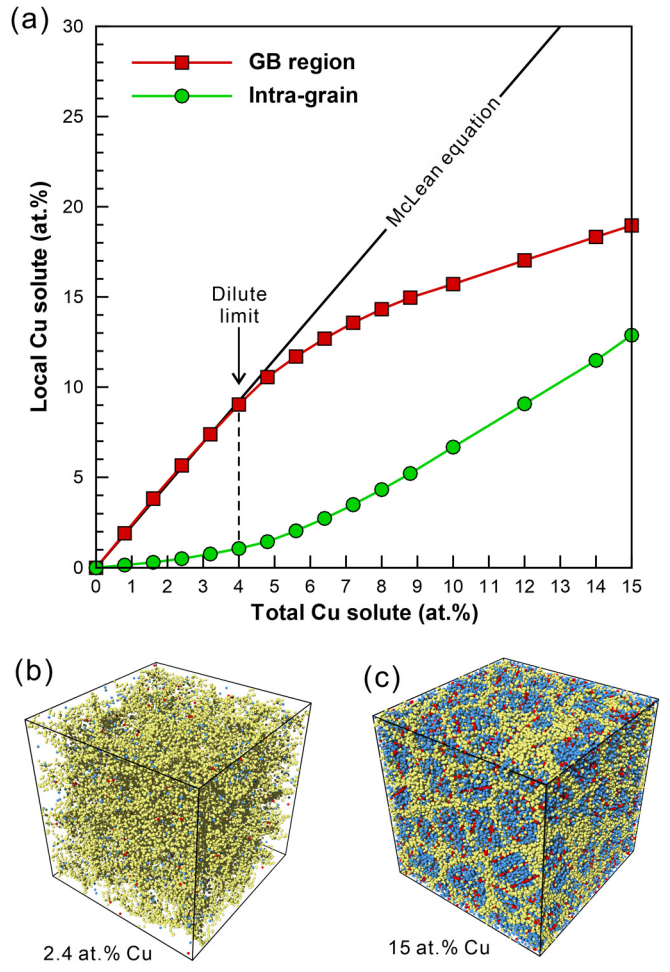

Fig. 6. (a) Local Cu concentration in GB network and grain interior, as a function of total solute content, in nanocrystalline Ag-Cu alloys with $d = 8$ nm. The classical McLean model from Eq. (7) is also shown for comparison. Equilibrium Cu solute distributions at (b) low solute content (2.4 at.%) and (c) high solute content (15.0 at.%.) Atoms in perfect FCC arrangement are colored in blue, coherent twin-boundaries in red color, and GBs in yellow color. (For interpretation of the references to colour in this figure legend, the reader is referred to the web version of this article.)

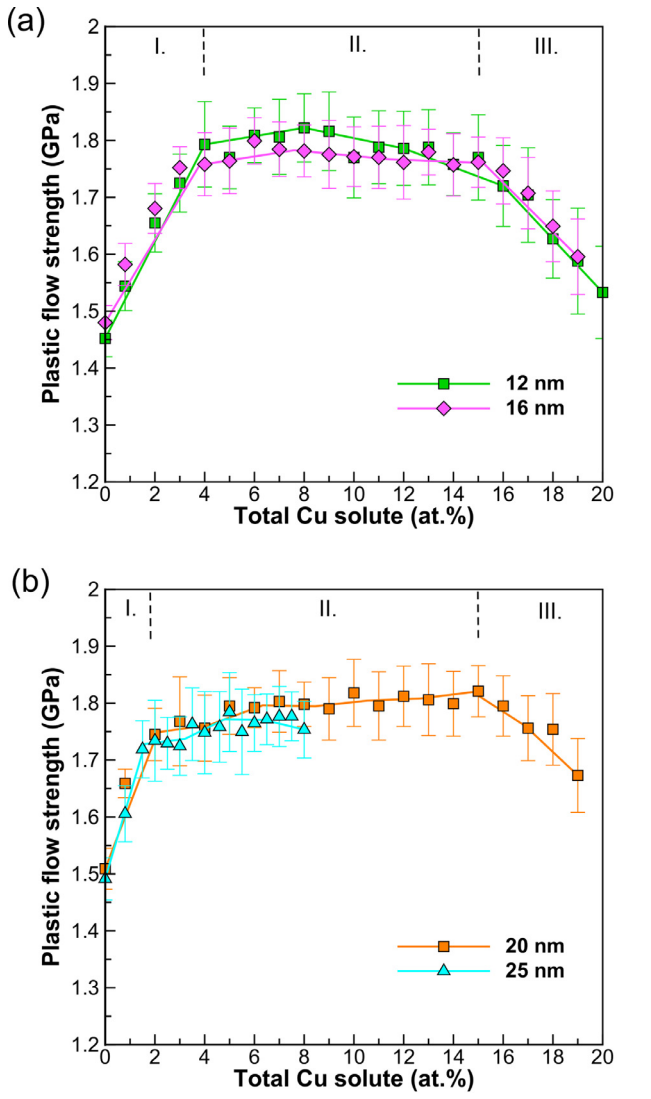

Fig. 7. Effects of total solute content on plastic flow strength in nanocrystalline Ag-Cu alloys with an average grain size of (a) 12 nm and 16 nm, and (b) 20 nm and 25 nm.

plies that GB atoms have larger free volume than intra-grain ones. Because atomic motion inside GBs can accommodate local stresses more easily due to volume expansion, any sign of nanoscale cavitation is absent, as indicated by the homogeneous volumetric strain at 10% strain without solute in Fig. 5(c).

However, we find in Fig. 5(d) that the EFV at GBs decreases linearly with the local GB solute content. Surprisingly, the EFV becomes negative above a local GB solute content of 18 at.%. This peculiar result stems from the pronounced reduction of free volume at GBs below that in the grains, as shown in Fig. 5(e) with a polycrystal containing 15 at.% Cu. Furthermore, the distribution of volumetric strain in Fig. 5(f) reveals important nanovoid expansion along the shear band predicted in Fig. 4(f) at 15 at.% Cu, contrasting with the homogeneous volumetric strain predicted in pure nc-Ag in Fig. 5(c). This behavior agrees well with micro-cracking mechanisms in hard and quasi-brittle metallic glasses induced by nanoscale cavitation and excess free volume inside localized amorphous shear bands [61]. Also, a body of evidence exists in the literature for preferential nucleation of nanoscale voids at GBs and GB triple junctions in tensile deformation of nanocrystalline metals [62–64].

A more detailed analysis of solute distribution between GB and grain interior in Fig. 6 offers some physical ground for interpreting the origin of a negative EFV at high Cu contents. The total solute content is divided between the average solute contents in the grain interior and the GB network, X^c and $\bar{X}^{GB}$, respectively, as function of the GB atom fraction by:

$$X^{tot} = (1 - f_{GB})X^c + f_{GB}\bar{X}^{GB} \tag{6}$$

In the dilute limit where solute concentration is assumed to be too low to cause solute interactions, the classical "average" thermodynamical approach by McLean [65] predicts the local solute content at GBs such as Eq. (7):

$$\bar{X}^{GB} = \left[1 + \frac{1 - X^c}{X^c} \exp\left(\frac{\Delta\bar{E}^{seg}}{kT}\right)\right] \tag{7}$$

where $\Delta\bar{E}^{seg}$ is the average solute segregation in the GB network, T is the temperature, and k is the Boltzmann constant. Fig. 6(a) shows that the McLean model with $d = 8$ nm, $f_{GB} = 0.37$, and $\Delta\bar{E}^{seg} = -0.12$ eV, agrees well with our MC/MD simulations up to a total solute content of 4 at.%, and stays within 9% error until 4.8 at.%. An atomic-scale snapshot of the Cu distribution in the polycrystal at 2.4 at.% in Fig. 6(b) indicates that majority of solute atoms are located inside GBs, which means that the EFV adheres well to Eq. (1).

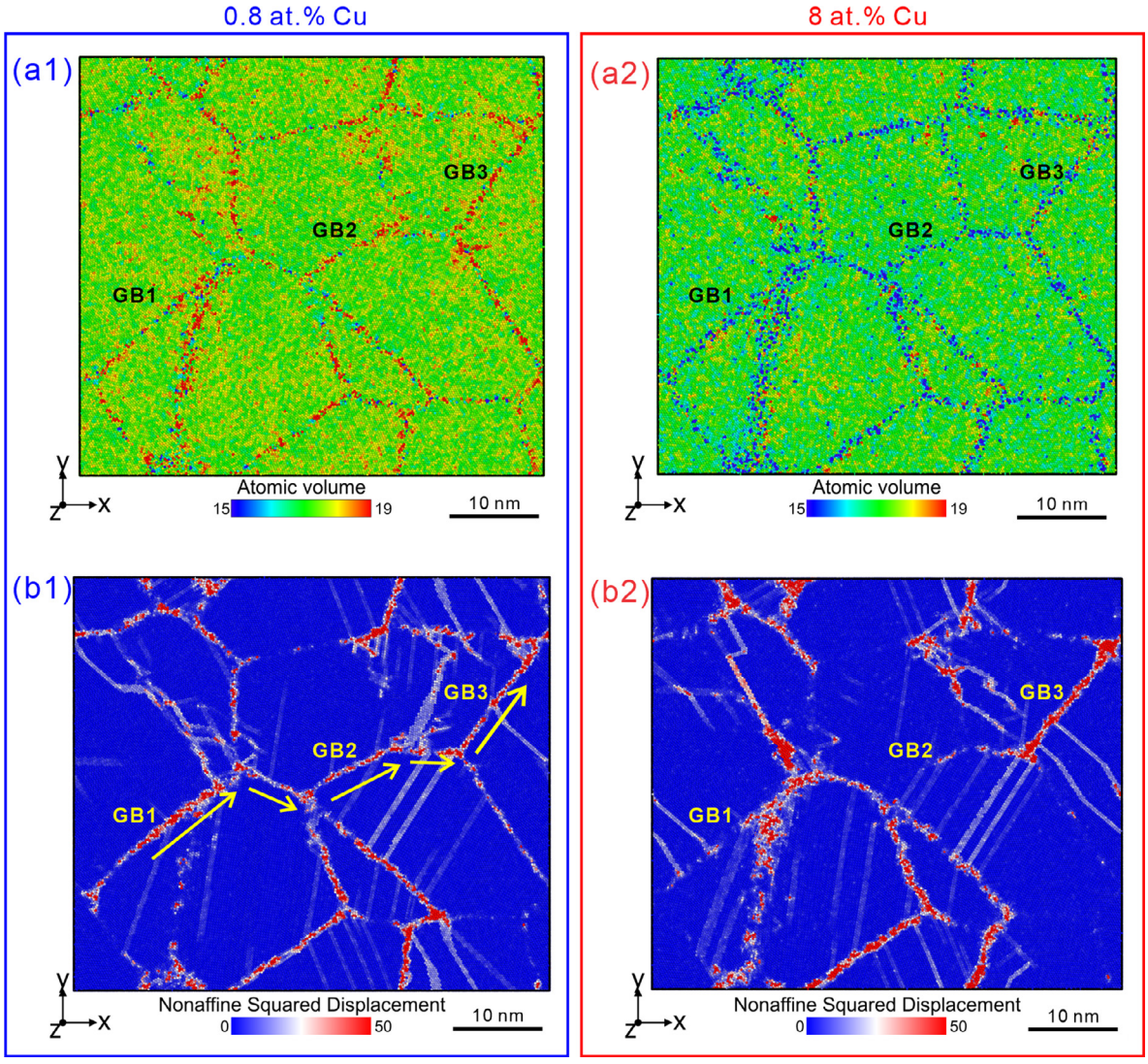

Fig. 8. Effects of solute content (0.8 at.% versus 8 at.%) on partially active grain-boundary segregation in nanocrystalline Ag-Cu alloys with $d = 20$ nm. (a1, a2) Distributions of atomic volume (Å^3) at 7% applied strain. (b1, b2) Maps of non-affine squared displacements (Å) computed in the strain range from 7 to 9.5%.

Above 6 at.% solute, however, a significant departure of the local GB solute content from the McLean model is clearly manifest in Fig. 6(a). This difference has been attributed by Wagih and Schuh [66] to the separate contributions of solute interactions beyond the dilute limit and a spectral distribution of segregation energies at GB atom sites in polycrystals. This behavior also relates to a recent study by Zhou et al. [67] on segregation behavior in nc Ni-P alloys where interfacial solute partitioning promotes Zener pinning mechanisms from nanoscale GB precipitates that start forming at 4 at.% phosphorous.

Furthermore, past atomistic simulations on Ag-doped Cu alloys [33] have predicted that solute segregates entirely to GBs to form a thick layer of Ag atoms at the interfaces at high concentrations, effectively leading to a perfectly wetting-film complexion [68]. However, our simulations in Fig. 6(c) suggest a different segregation mechanism at high solute content where Cu solute atoms are distributed uniformly in both GBs and grain interiors, with a preference to segregate to GBs, with no film formed at interfaces. After Cu segregation, majority of GB atoms are still Ag atoms, while significant amount of Cu remains in solution inside the grains. Quantitatively, Fig. 6(a) shows that, at a total Cu content of 14 at.%, the average local solute content is close, 18.3 at.% and 11.5 at.%, at the GBs and in the grain interior, respectively. Therefore, it is possible that the negative value of EFV at high solute concentration stems from a re-dissolution of solute inside grains, which has been observed previously in nc Ag-W alloys at elevated temperature [69].

3.4. Partially active segregation

A salient feature in this study is the occurrence of a zero-slope strength limit in nc Sterling silver, as a function of grain size, which could not be directly attributed to classical grain-size-dependent GB plasticity mechanisms. To elucidate this phenomenon, in Fig. 7, we systematically investigated the range of Cu solute contents over which the strengths reach a plateau at four different grain sizes, $d = 12$, 16, 20 and 25 nm. We find that the plateau regimes extend for concentrations from 4 at.% up to 15 at.% over the studied grain sizes. Interestingly, a limit of 4 at.% is significantly lower than the high solute contents found to form persistent shear bands, which suggests a third independent regime of plasticity between classical GB segregation strengthening and segregation-induced shear localization. Also, we can observe that at a grain size of $d = 8$ nm, the breakdown from classical GB segregation strengthening occurs at 6 at.% Cu in Fig. 3(b), whereas the dilute limit established at this grain size from McLean equation is only 4 at.% Cu in Fig. 6(a).

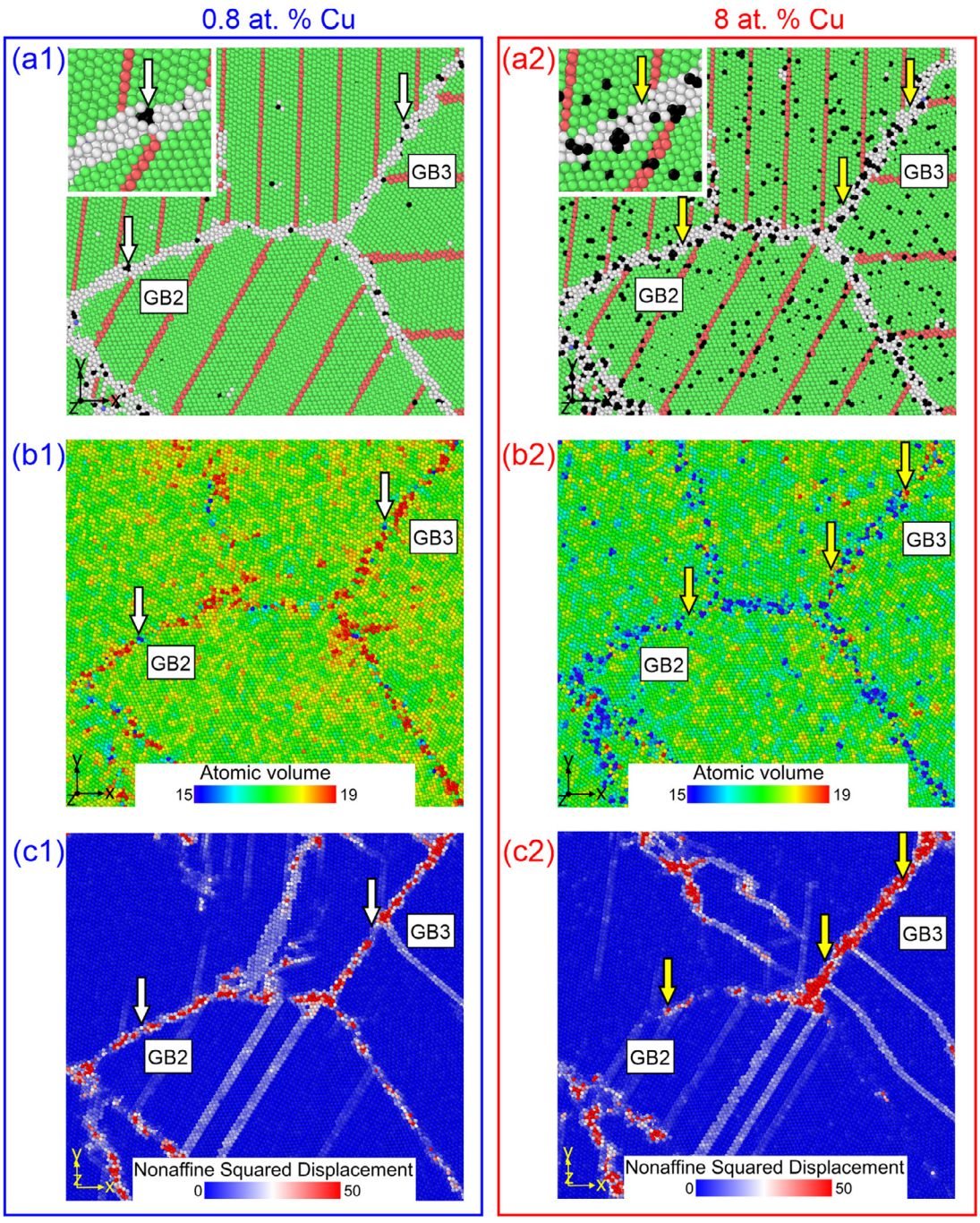

Fig. 9. Close-up views on local segregation and GB plasticity mechanisms at GB2 and GB3 interfaces in Fig. 8 for contents of 0.8 at.% Cu and 8 at.% Cu, respectively. (a1, a2) Local atom solute distributions. (b1, b2) Distributions of atomic volume ($Å^3$) at 7% applied strain. (c1, c2) Maps of non-affine squared displacements (Å) computed in the strain range from 7 to 9.5%.

Therefore, we hypothesize that the maximum strength plateau could relate to GB solute interactions. To verify this hypothesis, in Fig. 8, we compare the GB-mediated plasticity in two Ag polycrystals with same grain size $d = 20$ nm but an order of magnitude difference in Cu solute content, i.e., 0.8 at.% versus 8 at.%. The former concentration lies in the normal regime of segregation strengthening, whereas the latter is part of the abnormal strength plateau in Fig. 7. Fig. 8(a1) and (a2) confirm that the overall GB atom volume at 7% applied strain is either superior or inferior to the intra-grain atom volume at 0.8 at.% Cu and 8 at.% Cu, respectively. In parallel, we computed the non-affine squared displacements in the strain range from 7% to 9.5%, which generally helped us identify uncommon long-range plasticity processes at Ag interfaces, such as atom diffusion [70]. In comparison, Fig. 8(b1) and (b2) show that non-affine squared displacements are more homogeneously distributed along GB atoms at 0.8 at.% Cu than at 8 at.% Cu. For example, a path for shear flow created through several aligned GBs, noted as GB1, GB2 and GB3, is continuous at 0.8 at.% Cu in Fig. 8(b1) and becomes strongly discontinuous at 8 at.% in Fig. 8(b1) and 8(b2), respectively.

Fig. 9 specifically details the shear flow discontinuity emerging between GB2 and GB3, as the solute concentration increases. In Fig. 9(a1), at 0.8 at.% Cu, segregation leads to a homogeneous distribution of GB solute comprising some rare clusters of 3 Cu atoms

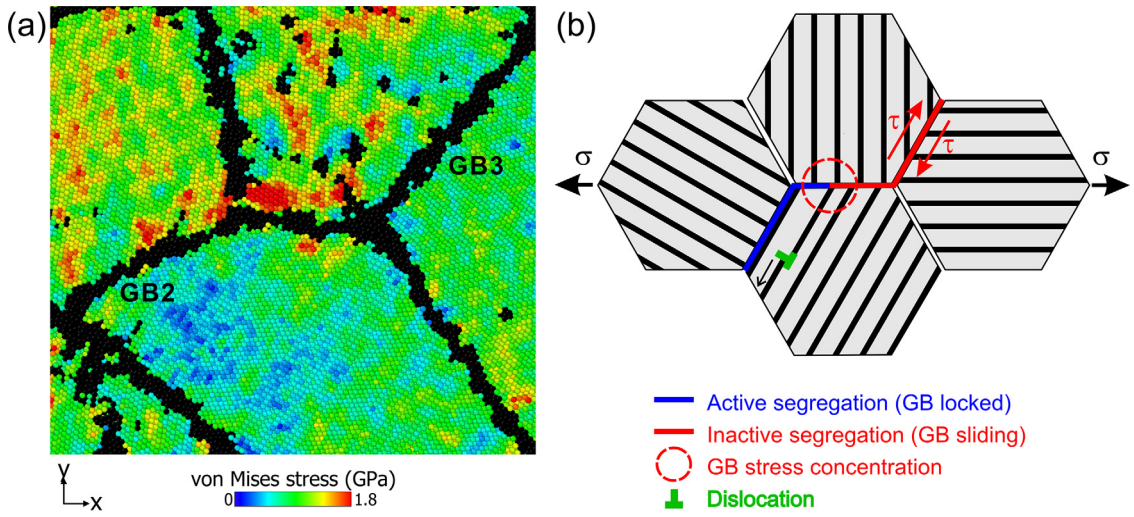

Fig. 10. (a) Atomic von Mises stresses at interfaces GB2 and GB3 for a total strain of 10%. The overall tensile flow stress is 1.789 GPa, which corresponds to the value of the GB stress concentrations resulting from sliding of GB3. (b) Schematic illustration of a GB stress concentration stemming from partially active segregation across GB interfaces.

in the boundaries. Fig. 9(b1) indicates that the atomic volume of those nanoclusters is smaller than that of GB atoms, causing the GB regions around them to exhibit relatively reduced shear flow, as observed by the white arrows in Fig. 9(c1). In the following, we refer to this as *partially active segregation*. However, since the solute interaction and nanocluster formation are limited below the dilute limit of 4 at.%, a continuous shear flow path is essentially maintained along the interfaces. On the contrary, the partially active segregation effect is dramatically amplified at 8 at.% Cu. In Fig. 9(a2), the GB2 and GB3 interfaces are more covered by Cu nanoclusters. While the size of GB clusters remains small (3–4 atoms), their density is more significant. The GB cluster distribution decreases the overall atomic volume in most GB regions but interestingly, not all regions, like those highlighted by yellow arrows in Fig. 9(b2). We attribute this phenomenon to the saturation of the local GB solute content as the solute concentration increases in Fig. 6(a). Recent theoretical studies on solute segregation in bicrystals and polycrystals [28,66,71] have proposed that GB solutes tend to first segregate to atomic GB sites associated with the highest local segregation energies, which facilitates solute-solute interaction at those specific GB sites. This theory therefore implies that there could be atomic GB sites with a lower segregation energy that are always less favorable for cluster formation, thereby rendering GB segregation locally inactive. In fact, similar local competition for solute segregation between different GBs of a polycrystal was evidenced in a recent atomistic simulation study on nc Cu-Zr alloys by Garg et al. [72]. In Fig. 9(b2), our simulation demonstrates this hypothesis because GB3 contains more inactive sites with positive (red) atom volume that GB2. Consequently, as found in Fig. 9(c2), the shear flow at GB2 is abruptly interrupted in the center of the interface at 8 at.% Cu (i.e. GB2 is locked), whereas shear flow in GB3 is more intensified (i.e. GB3 is sliding) due to partially inactive segregation.

To understand the relationship between partially active segregation and the constant strength plateau seen in Fig. 7, we propose to consider the effect of a shear flow discontinuity at GBs on the emergence of GB stress concentrations. For that purpose, in Fig. 10(a), we have computed the atomic-level von-Mises stresses at the end of our simulation (10% strain) with the model containing 8 at.% Cu. Fig. 10(a) reveals GB stress concentrations near the interface GB2, while the stresses surrounding the GB3 interface are more uniform. In fact, it is worth noting that the magnitude of the GB stress concentrations at GB 2 (~1.8 GPa) matches well with the maximum flow strengths in the plateau in Fig. 7. These GB stress concentrations are found to be the source for nucleation of partial dislocations in the adjacent grains, which is consistent with our previous observation in Fig. 4(e) showing that dislocation plasticity became more predominant than GB sliding as the solute content was increased to 8 at.% Cu.

A simple mechanistic model is proposed in Fig. 10(b) based on an idea by Asaro and Suresh [73] for predicting dislocation nucleation from GBs in nc metals. They derived the effective stress intensity K^{crit} to nucleate a lead partial dislocation from a GB stress concentration in nc metals based on the Peierls framework [74], such as

$$K^{crit} = \sqrt{\frac{2\mu\gamma_{US}}{(1-\nu)}} \tag{8}$$

where μ and ν are the shear modulus and Poisson's ratio, respectively, and γ_{US} is the unstable stacking-fault energy. In our model, interfaces dominated by inactive segregation such as GB3 are viewed as being plastically deformed by shear-induced sliding as illustrated in Fig. 10(b), similarly to the behavior of a crack under pure shear mode. A stress intensity is created where the deformation in the next interface, such as GB2, is locked due to active segregation. As the GB stress intensity increases to K^{crit}, a dislocation nucleates in an adjacent grain. From Eq. (8), it is evident that K^{crit} is independent on the solute concentration because μ, ν and γ_{US} are not expected to vary significantly for Cu solute $<$ 20 at.%. This conclusion is supported by the fact that, in our past simulation study [17], no solid solution effect were found on the generalized stacking-fault energy curve of Ag-Cu alloys with Cu solute up to 5 at.%. Therefore, our model provides some mechanistic ground for interpreting the occurrence of constant strengths, as a function of solute concentration, in nc Sterling silver, owing to dislocation nucleation mechanisms from GB stress concentrations induced by partially active segregation.

4. Conclusion

Large-scale hybrid MC/MD simulations have been used to study the effects of grain size and Cu content on Hall–Petch breakdown mechanisms in silver alloys containing less than 20 at.% Cu. We have identified three concentration-dependent regimes of plasticity that are directly influenced by GB solute segregation: (1) Classical segregation strengthening behavior at low solute contents, (2) shear band-induced softening at high solute contents, and (3) an extended plateau of maximum strengths for intermediate solute

contents from 4 to 15 at.%, which we term as nc Sterling silver. It was found that the excess free volume at GBs decreases linearly with the local GB solute content, leading to the GB segregation strengthening effect. Surprisingly, the excess volume becomes negative above a local GB solute content of 18 at.% in Ag-Cu alloys. Important nanovoid expansion along persistent shear bands are predicted at solute content above 15 at% Cu, leading to strain-localization-induced softening. In nc Sterling silver with Cu solute contents between 4 and 15 at.%, a plateau of maximum strengths that is below the ideal Hall–Petch limit, was observed for all grain sizes equal to or less than 20 nm. The concentration-independent strength limit in nc Sterling silver resulted from the emergence of GB stress concentrations induced by partially active segregation effects that act to influence interfacial plasticity in some, but not all, GB regions. In the case of Ag-Cu alloys, solute-solute interaction and the distribution of solute nanoclusters at GBs were found responsible for this phenomenon. In more general, these conclusions are relevant for all types of nanocrystalline alloys stabilized by GB solute segregation above their dilute limit.

Declaration of Competing Interest

The authors declare that they have no known competing financial interests or personal relationships that could have appeared to influence the work reported in this paper.

Acknowledgment

We gratefully thank support from the U.S. Department of Energy (DOE) Grants Nos. DE-SC0016270 and DE-SC0020054. This research used the computational resources provided by the NERSC, a DOE Office of Science User Facility under Contract No. DE-AC02-05CH11231, and XSEDE, which is supported by the National Science Foundation under Grant No. ACI-1548562.

References

[1] S. Yip, The strongest size, Nature 391 (6667) (1998) 532–533.
[2] E.O. Hall, The deformation and ageing of mild steel: III discussion of results, Proc. Phys. Soc. Lond. Sect. B 64 (1951) 747.
[3] N. Petch, The cleavage strength of polycrystals, J. Iron Steel Inst. 174 (1953) 25–28.
[4] F.D.D.T. Jakob Schiøtz, K.W. Jacobsen, Softening of nanocrystalline metals at very small grain sizes, Nature 391 (6667) (1998) 561–563.
[5] H. Van Swygenhoven, P. Derlet, Grain-boundary sliding in nanocrystalline FCC metals, Phys. Rev. B 64 (22) (2001) 224105.
[6] T. Rupert, D. Gianola, Y. Gan, K. Hemker, Experimental observations of stress–driven grain boundary migration, Science 326 (5960) (2009) 1686–1690.
[7] K. Zhang, J.R. Weertman, J.A. Eastman, Rapid stress-driven grain coarsening in nanocrystalline Cu at ambient and cryogenic temperatures, Appl. Phys. Lett. 87 (6) (2005) 061921.
[8] F. Sansoz, V. Dupont, Grain growth behavior at absolute zero during nanocrystalline metal indentation, Appl. Phys. Lett. 89 (11) (2006) 111901.
[9] A. Detor, C. Schuh, Grain boundary segregation, chemical ordering and stability of nanocrystalline alloys: atomistic computer simulations in the Ni–W system, Acta Mater. 55 (12) (2007) 4221–4232.
[10] A. Caro, D. Farkas, E. Bringa, G. Gilmer, L. Zepeda-Ruiz, Effects of microalloying on the mobility and mechanical response of interfaces in nanocrystalline Cu, Mater. Sci. Forum Trans. Tech. Publ. (2010) 21–30.
[11] J. Schäfer, A. Stukowski, K. Albe, Plastic deformation of nanocrystalline Pd–Au alloys: on the interplay of grain boundary solute segregation, fault energies and grain size, Acta Mater. 59 (8) (2011) 2957–2968.
[12] N.Q. Vo, J. Schafer, R.S. Averback, K. Albe, Y. Ashkenazy, P. Bellon, Reaching theoretical strengths in nanocrystalline Cu by grain boundary doping, Scr. Mater. 65 (8) (2011) 660–663.
[13] J. Schafer, K. Albe, Plasticity of nanocrystalline alloys with chemical order: on the strength and ductility of nanocrystalline Ni-Fe, Beilstein J. Nanotechnol. 4 (2013) 542–553.
[14] P. Zhang, J.Y. Zhang, J. Li, G. Liu, K. Wu, Y.Q. Wang, J. Sun, Microstructural evolution, mechanical properties and deformation mechanisms of nanocrystalline Cu thin films alloyed with Zr, Acta Mater. 76 (2014) 221–237.
[15] Y. Zhang, G.J. Tucker, J.R. Trelewicz, Stress-assisted grain growth in nanocrystalline metals: grain boundary mediated mechanisms and stabilization through alloying, Acta Mater. 131 (2017) 39–47.
[16] S.C. Pun, W.B. Wang, A. Khalajhedayati, J.D. Schuler, J.R. Trelewicz, T.J. Rupert, Nanocrystalline Al-Mg with extreme strength due to grain boundary doping, Mater. Sci. Eng. A Struct. 696 (2017) 400–406.
[17] X. Ke, F. Sansoz, Segregation-affected yielding and stability in nanotwinned silver by microalloying, Phys. Rev. Mater. 1 (6) (2017) 063604.
[18] X. Ke, J. Ye, Z. Pan, J. Geng, M.F. Besser, D. Qu, A. Caro, J. Marian, R.T. Ott, Y.M. Wang, F. Sansoz, Ideal maximum strengths and defect-induced softening in nanocrystalline-nanotwinned metals, Nat. Mater. 18 (11) (2019) 1207–1214.
[19] J. Schafer, Y. Ashkenazy, K. Albe, R.S. Averback, Effect of solute segregation on thermal creep in dilute nanocyrstalline Cu alloys, Mater. Sci. Eng. A Struct. 546 (2012) 307–313.
[20] M. Kapoor, T. Kaub, K.A. Darling, B.L. Boyce, G.B. Thompson, An atom probe study on Nb solute partitioning and nanocrystalline grain stabilization in mechanically alloyed Cu-Nb, Acta Mater. 126 (2017) 564–575.
[21] J. Hu, Y.N. Shi, X. Sauvage, G. Sha, K. Lu, Grain boundary stability governs hardening and softening in extremely fine nanograined metals, Science 355 (6331) (2017) 1292–1296.
[22] A. Gupta, J. Gruber, S.S. Rajaram, G.B. Thompson, D.L. McDowell, G.J. Tucker, On the mechanistic origins of maximum strength in nanocrystalline metals, NPJ Comput. Mater. 6 (1) (2020) 153.
[23] C.A. Schuh, T.G. Nieh, H. Iwasaki, The effect of solid solution W additions on the mechanical properties of nanocrystalline Ni, Acta Mater. 51 (2) (2003) 431–443.
[24] A. Giga, Y. Kimoto, Y. Takigawa, K. Higashi, Demonstration of an inverse Hall–Petch relationship in electrodeposited nanocrystalline Ni–W alloys through tensile testing, Scr. Mater. 55 (2) (2006) 143–146.
[25] Y. Zhou, U. Erb, K.T. Aust, G. Palumbo, The effects of triple junctions and grain boundaries on hardness and Young's modulus in nanostructured Ni–P, Scr. Mater. 48 (6) (2003) 825–830.
[26] D.H. Jeong, U. Erb, K.T. Aust, G. Palumbo, The relationship between hardness and abrasive wear resistance of electrodeposited nanocrystalline Ni–P coatings, Scr. Mater. 48 (8) (2003) 1067–1072.
[27] F. Sansoz, K.D. Stevenson, Relationship between hardness and dislocation processes in a nanocrystalline metal at the atomic scale, Phys. Rev. B 83 (22) (2011) 224101.
[28] M. Wagih, P.M. Larsen, C.A. Schuh, Learning grain boundary segregation energy spectra in polycrystals, Nat. Commun. 11 (1) (2020) 6376.
[29] S. Ozerinc, K.P. Tai, N.Q. Vo, P. Bellon, R.S. Averback, W.P. King, Grain boundary doping strengthens nanocrystalline copper alloys, Scr. Mater. 67 (7–8) (2012) 720–723.
[30] H.W. Zhang, K. Lu, R. Pippan, X. Huang, N. Hansen, Enhancement of strength and stability of nanostructured Ni by small amounts of solutes, Scr. Mater. 65 (6) (2011) 481–484.
[31] K.S. Kormout, B. Yang, R. Pippan, Deformation behavior and microstructural evolution of Cu–Ag alloys processed by high-pressure torsion, Adv. Eng. Mater. 17 (12) (2015) 1828–1834.
[32] G.H. Balbus, F. Wang, D.S. Gianola, Suppression of shear localization in nanocrystalline Al–Ni–Ce via segregation engineering, Acta Mater. 188 (2020) 63–78.
[33] A. Li, I. Szlufarska, Morphology and mechanical properties of nanocrystalline Cu/Ag alloy, J. Mater. Sci. 52 (8) (2017) 4555–4567.
[34] Q. Li, J. Zhang, H. Tang, H. Ye, Y. Zheng, Regulating the mechanical properties of nanocrystalline nickel via molybdenum segregation: an atomistic study, Nanotechnology 30 (27) (2019) 275702.
[35] R.T. Ott, J. Geng, M.F. Besser, M.J. Kramer, Y.M. Wang, E.S. Park, R. LeSar, A.H. King, Optimization of strength and ductility in nanotwinned ultra-fine grained Ag: twin density and grain orientations, Acta Mater. 96 (2015) 378–389.
[36] N.P. Kobelev, Y.M. Soifer, R.A. Andrievski, B. Gunther, Microhardness and elastic properties of nanocrystalline silver, Nanostruct. Mater. 2 (5) (1993) 537–544.
[37] X.Y. Qin, X.J. Wu, L.D. Zhang, The microhardness of nanocrystalline silver, Nanostruct. Mater. 5 (1) (1995) 101–110.
[38] H. Conrad, K. Jung, Effect of grain size from millimeters to nanometers on the flow stress and deformation kinetics of Ag, Mater. Sci. Eng. A 391 (1) (2005) 272–284.
[39] T. Kizuka, H. Ichinose, Y. Ishida, Structure and hardness of nanocrystalline silver, J. Mater. Sci. 32 (6) (1997) 1501–1507.
[40] S. Plimpton, Fast parallel algorithms for short-range molecular-dynamics, J. Comput. Phys. 117 (1) (1995) 1–19.
[41] H.H. Wu, D.R. Trinkle, Cu/Ag EAM potential optimized for heteroepitaxial diffusion from Ab initio data, Comput. Mater. Sci. 47 (2) (2009) 577–583.
[42] A. Stukowski, Visualization and analysis of atomistic simulation data with OVITO–the open visualization tool, modeling and simulation, Mater. Sci. Eng. 18 (1) (2010) 015012.
[43] G. Voronoi, Nouvelles applications des paramétres continus á la théorie des formes quadratiques, deuxiéme mémoire, recherches sur les paralléloédres primitifs, J. für Reine Angew. Math. 138 (1908) 198–287.
[44] J. Towns, T. Cockerill, M. Dahan, I. Foster, K. Gaither, A. Grimshaw, V. Hazlewood, S. Lathrop, D. Lifka, G.D. Peterson, R. Roskies, J.R. Scott, N. Wilkins-Diehr, XSEDE: accelerating scientific discovery, Comput. Sci. Eng. 16 (5) (2014) 62–74.
[45] K. Ishida, Effect of grain size on grain boundary segregation, J. Alloy. Compd. 235 (2) (1996) 244–249.
[46] J.R. Trelewicz, C.A. Schuh, Grain boundary segregation and thermodynamically stable binary nanocrystalline alloys, Phys. Rev. B 79 (9) (2009) 094112.
[47] M. Chandross, N. Argibay, Ultimate strength of metals, Phys. Rev. Lett. 124 (12) (2020) 125501.

[48] Z. Pan, V. Borovikov, M.I. Mendelev, F. Sansoz, Development of a semi-empirical potential for simulation of Ni solute segregation into grain boundaries in Ag, modeling and simulation in, Mater. Sci. Eng. 26 (7) (2018) 075004.
[49] K. Youssef, M. Sakaliyska, H. Bahmanpour, R. Scattergood, C. Koch, Effect of stacking fault energy on mechanical behavior of bulk nanocrystalline Cu and Cu alloys, Acta Mater. 59 (14) (2011) 5758–5764.
[50] J.C.M. Li, Petch relation and grain boundary sources, Trans. Metall. Soc. AIME 227 (1) (1963) 239.
[51] H. Lüthy, R.A. White, O.D. Sherby, Grain boundary sliding and deformation mechanism maps, Mater. Sci. Eng. 39 (2) (1979) 211–216.
[52] L. Slifkin, D. Lazarus, T. Tomizuka, Self-diffusion in pure polycrystalline silver, J. Appl. Phys. 23 (9) (1952) 1032–1034.
[53] D.A. Jones, A.F. Jankowski, G.A. Davidson, Room-temperature diffusion in Cu/Ag thin-film couples caused by anodic dissolution, Metall. Mater. Trans. A 28 (13) (1997) 843–850.
[54] I. Baker, in: Silver, Fifty Materials That Make the World, Springer, 2018, pp. 211–214.
[55] C. Schuh, Deadlocked order and disorder in the strongest metals, Physics 13 (2020) 42.
[56] R.K. Koju, Y. Mishin, Relationship between grain boundary segregation and grain boundary diffusion in Cu-Ag alloys, Phys. Rev. Mater. 4 (7) (2020) 073403.
[57] H. Van Swygenhoven, P.M. Derlet, Grain-boundary sliding in nanocrystalline FCC metals, Phys. Rev. B 64 (22) (2001).
[58] H. Van Swygenhoven, P.M. Derlet, A. Hasnaoui, Atomic mechanism for dislocation emission from nanosized grain boundaries, Phys. Rev. B 66 (2) (2002).
[59] F. Sansoz, J.F. Molinari, Incidence of atom shuffling on the shear and decohesion behavior of a symmetric tilt grain boundary in copper, Scr. Mater. 50 (10) (2004) 1283–1288.
[60] F. Sansoz, J.F. Molinari, Mechanical behavior of Σ tilt grain boundaries in nanoscale Cu and Al: a quasicontinuum study, Acta Mater. 53 (7) (2005) 1931–1944.
[61] C.A. Schuh, T.C. Hufnagel, U. Ramamurty, Mechanical behavior of amorphous alloys, Acta Mater. 55 (12) (2007) 4067–4109.
[62] A. Hasnaoui, H. Van Swygenhoven, P.M. Derlet, Dimples on nanocrystalline fracture surfaces as evidence for shear plane formation, Science 300 (5625) (2003) 1550.
[63] P. Noell, J. Carroll, K. Hattar, B. Clark, B. Boyce, Do voids nucleate at grain boundaries during ductile rupture? Acta Mater. 137 (2017) 103–114.
[64] Q. Fang, F. Sansoz, Columnar grain-driven plasticity and cracking in nanotwinned FCC metals, Acta Mater. 212 (2021) 116925.
[65] D. McLean, Grain Boundaries in Metals, Clarendon Press, Oxford, 1957.
[66] M. Wagih, C.A. Schuh, Grain boundary segregation beyond the dilute limit: separating the two contributions of site spectrality and solute interactions, Acta Mater. 199 (2020) 63–72.
[67] X. Zhou, A. Gupta, G.J. Tucker, G.B. Thompson, Manipulation of solute partitioning mechanisms for nanocrystalline stability, Acta Mater. 208 (2021) 116662.
[68] S.J. Dillon, M. Tang, W.C. Carter, M.P. Harmer, Complexion: a new concept for kinetic engineering in materials science, Acta Mater. 55 (18) (2007) 6208–6218.
[69] Z. Jiao, C. Schuh, Nanocrystalline Ag-W alloys lose stability upon solute desegregation from grain boundaries, Acta Mater. 161 (2018) 194–206.
[70] L. Zhong, F. Sansoz, Y. He, C. Wang, Z. Zhang, S.X. Mao, Slip-activated surface creep with room-temperature super-elongation in metallic nanocrystals, Nat. Mater. 16 (4) (2017) 439–445.
[71] L. Huber, R. Hadian, B. Grabowski, J. Neugebauer, A machine learning approach to model solute grain boundary segregation, NPJ Comput. Mater. 4 (1) (2018) 64.
[72] P. Garg, Z. Pan, V. Turlo, T.J. Rupert, Segregation competition and complexion coexistence within a polycrystalline grain boundary network, Acta Mater. 218 (2021) 117213.
[73] R.J. Asaro, S. Suresh, Mechanistic models for the activation volume and rate sensitivity in metals with nanocrystalline grains and nano-scale twins, Acta Mater. 53 (12) (2005) 3369–3382.
[74] J.R. Rice, Dislocation nucleation from a crack tip: an analysis based on the Peierls concept, J. Mech. Phys. Solids 40 (2) (1992) 239–271.